

## Improvements to Lake-Effect Snow Forecasts Using a One-Way Air–Lake Model Coupling Approach

AYUMI FUJISAKI-MANOME,<sup>a,b</sup> GREG E. MANN,<sup>c</sup> ERIC J. ANDERSON,<sup>d</sup> PHILIP Y. CHU,<sup>d</sup> LINDSAY E. FITZPATRICK,<sup>a</sup> STANLEY G. BENJAMIN,<sup>e</sup> ERIC P. JAMES,<sup>e,f</sup> TATIANA G. SMIRNOVA,<sup>e,f</sup> CURTIS R. ALEXANDER,<sup>e</sup> AND DAVID M. WRIGHT<sup>b</sup>

<sup>a</sup> Cooperative Institute for Great Lakes Research, University of Michigan, Ann Arbor, Michigan; <sup>b</sup> Climate and Space Sciences and Engineering, University of Michigan, Ann Arbor, Michigan; <sup>c</sup> NOAA/National Weather Service/Detroit Weather Forecast Office, White Lake, Michigan; <sup>d</sup> NOAA/Great Lakes Environmental Research Laboratory, Ann Arbor, Michigan; <sup>e</sup> NOAA/Earth System Research Laboratory, Boulder, Colorado; <sup>f</sup> Cooperative Institute for Research in Environmental Sciences, University of Colorado Boulder, Boulder, Colorado

(Manuscript received 31 March 2020, in final form 17 August 2020)

**ABSTRACT:** Lake-effect convective snowstorms frequently produce high-impact, hazardous winter weather conditions downwind of the North American Great Lakes. During lake-effect snow events, the lake surfaces can cool rapidly, and in some cases, notable development of ice cover occurs. Such rapid changes in the lake-surface conditions are not accounted for in existing operational weather forecast models, such as the National Oceanic and Atmospheric Administration's (NOAA) High-Resolution Rapid Refresh (HRRR) model, resulting in reduced performance of lake-effect snow forecasts. As a milestone to future implementations in the Great Lakes Operational Forecast System (GLOFS) and HRRR, this study examines the one-way linkage between the hydrodynamic-ice model [the Finite-Volume Community Ocean Model coupled with the unstructured grid version of the Los Alamos Sea Ice Model (FVCOM-CICE), the physical core model of GLOFS] and the atmospheric model [the Weather Research and Forecasting (WRF) Model, the physical core model of HRRR]. The realistic representation of lake-surface cooling and ice development or its fractional coverage during three lake-effect snow events was achieved by feeding the FVCOM-CICE simulated lake-surface conditions to WRF (using a regional configuration of HRRR), resulting in the improved simulation of the turbulent heat fluxes over the lakes and resulting snow water equivalent in the downwind areas. This study shows that the one-way coupling is a practical approach that is well suited to the operational environment, as it requires little to no increase in computational resources yet can result in improved forecasts of regional weather and lake conditions.

**KEYWORDS:** Inland seas/lakes; Lake effects; Boundary layer; Snowfall; Operational forecasting; Numerical weather prediction/forecasting

### 1. Introduction

Severe winter weather events involving ice and snow kill dozens of people every year around the Great Lakes region and impact a wide range of socioeconomic activities, such as commercial shipping, winter recreation, transportation, and utilities (e.g., Lake Carriers' Association 2019; Ayon 2017; Niziol 1987). Accurate and timely forecasts of hazardous winter weather are critical for safety and support mitigation activities intended to reduce associated losses. However, numerical weather and lake models require further refinements in order to improve these forecasts (Prasad et al. 2010; Samenow 2019). In the Great Lakes region, hazardous

winter weather is often associated with cold air outbreaks originating from the Arctic region. For example, lake-effect snow (LES) bands and resulting snowfall are common mesoscale convective weather phenomena in the Great Lakes region during the late autumn and throughout the winter (Cordeira and Laird 2008; Vavrus et al. 2013; Notaro et al. 2013). LES is primarily driven by the large vertical temperature gradient imposed on the atmospheric surface layer by forcing a cold air mass over a relatively warm lake surface. The morphology of mesoscale lake-effect structures was found to have distinct types, which are documented in Kristovich et al. (2003). In any case, the induced fluxes of moisture and heat from the lake surface provide buoyancy to the air above the lake, ultimately producing cloud bands and the potential for precipitation in the form of rain or snowfall over the water and downwind landmass. These fluxes of moisture and heat are sensitive to changes in lake ice. Latent heat fluxes off the lake surface have been shown to decrease relatively linearly with increases in ice coverage while sensible heat fluxes are constant until about 70% spatial ice coverage, after which sensible heat fluxes decrease rapidly (Gerbush et al. 2008).

It remains a challenge for numerical weather models to accurately forecast the timing, location, and intensity of LES storms

Denotes content that is immediately available upon publication as open access.

Supplemental information related to this paper is available at the Journals Online website: <https://doi.org/10.1175/JHM-D-20-0079.s1>.

Corresponding author: Ayumi Fujisaki-Manome, ayumif@umich.edu

DOI: 10.1175/JHM-D-20-0079.1

© 2020 American Meteorological Society. For information regarding reuse of this content and general copyright information, consult the AMS Copyright Policy ([www.ametsoc.org/PUBSReuseLicenses](http://www.ametsoc.org/PUBSReuseLicenses)).

due to the complexity of the process. Prior numerical modeling studies show that predictions of LES are notably influenced by lake ice cover (Wright et al. 2013), mean lake temperature (Hjelmfelt and Braham 1983; Theeuwes et al. 2010), atmosphere–lake temperature differences (Laird et al. 2003), lake surface temperature variations (Shi and Xue 2019), cloud microphysics parameterizations (Theeuwes et al. 2010; Reeves and Dawson 2013), and parameterizations of planetary and surface boundary layers (Conrick et al. 2015; Minder et al. 2020). These previous studies collectively indicate that the turbulent heat fluxes (i.e., heat and moisture fluxes from the lakes) are critical factors that need to be represented well in the models to accurately simulate LES bands. Fujisaki-Manome et al. (2017) showed that operational forecast models present high uncertainty in turbulent sensible and latent heat fluxes over Lake Erie (i.e., heat and moisture loss from the lake surface) for a record LES event over Buffalo, New York, in November 2014. In atmospheric models, the uncertainty is partly caused by oversimplified surface boundary conditions via the prescription of temporally constant, satellite-based lake-surface temperatures and ice cover over the forecast horizon. Having temporally static lake-surface conditions from satellite analyses is the default configuration in the vast majority of short-term weather forecast model applications, such as the High-Resolution Rapid Refresh (HRRR; Benjamin et al. 2016a,b), which runs hourly at the National Oceanic and Atmospheric Administration (NOAA) Centers for Environmental Prediction (NCEP). Reasonable performance can be expected when lake-surface conditions are relatively static. In the climatological seasonal cycle, this is likely the case as the estimated climatological cooling rates of lake-wide mean surface temperature during November–December ranged for  $0.5^{\circ}$ – $1.5^{\circ}\text{C week}^{-1}$  across the Great Lakes (Fichot et al. 2019), providing a cooling rate of  $0.07^{\circ}$ – $0.21^{\circ}\text{C day}^{-1}$ . However, in episodic storm events in fall and early winter, the lake surface can cool at a faster rate, especially in shallow lakes where thermal inertia is relatively small. For example, based on Fujisaki-Manome et al. (2017), the lake-wide mean surface temperature in Lake Erie cooled down by  $0.6^{\circ}$ – $1.0^{\circ}\text{C day}^{-1}$  during the LES storm in November 2014. Cooling rates of the lake surface temperature in the other Great Lakes in responding to a storm event are not well documented. However, given that the climatological cooling rates in fall and early winter were estimated to be similar among the Great Lakes in contrast with the large variation of the warming rates in spring and summer (Fichot et al. 2019), Lake Erie may not be the only lake where a rapid cooling of the lake surface occurs and where the static lake-surface conditions are not appropriate. Another concern with the lake-surface conditions currently used in weather forecast models is that they are often based on satellite measurements that could be out of date by several days due to persistent cloud cover leading to erroneous results. Given that the sensitivity was demonstrated previously in numerical simulations of LES to changes in the lake–atmosphere temperature differences on the order of a few degrees Celsius (Laird et al. 2003; Wright et al. 2013), it is important to account for the temporal evolution of lake-surface conditions.

When LES occurs late in the season, lake ice introduces further complexity into the system. Ice formation on the Great

Lakes occurs each year beginning in early December and lasts until late spring (Assel et al. 2003; Wang et al. 2018). In addition to presenting obstacle for mariners and vessels navigating the lakes, Great Lakes ice cover reduces the air–water transfer of heat and moisture and modifies wind stresses altering LES-band behavior (Cordeira and Laird 2008; Wright et al. 2013; Vavrus et al. 2013). Therefore, when considering dynamic evolution of lake-surface conditions during LES events, it is critical to provide accurate representation of ice cover on the lakes.

Currently, the first-ever short-term ice forecast for the Great Lakes is being developed to be incorporated to the existing NOAA’s Great Lakes Operational Forecast System (GLOFS; Anderson et al. 2018). This forecast model is based on a coupled ice–hydrodynamic model from the unstructured grid version of the Los Alamos Sea Ice Model (UG-CICE; Gao et al. 2011; Hunke et al. 2015) and the unstructured grid Finite Volume Community Ocean Model (FVCOM; Chen et al. 2006, 2013). The model is driven by prescribed surface meteorology from HRRR forecasts. Given that both HRRR and GLOFS provide operational NOAA forecasts, linking these weather, ice, and hydrodynamic models is one way to enable the modeling suite to exchange rapidly changing lake-surface conditions during LES events; thereby improving forecast accuracy.

The coupling of simplified parameterizations of lakes in numerical weather predictions has been increasing due to the reasonable performance and computational efficiency of these parameterizations (Mironov et al. 2010), but a large portion of the work has been focused on regional climate simulations with one-dimensional lake models (Mallard et al. 2014). Coupled the Advanced Research version of the Weather Research and Forecasting (WRF-ARW) Model (Skamarock et al. 2008) with the one-dimensional hydrodynamic Freshwater Lake (FLake; Mironov 2008) model to dynamically downscale climate simulations to allow for more explicit representation of the lakes and lake ice within the modeling system during the winter season. Their study used a 12-km horizontal resolution domain over the Great Lakes and found better simulations of the onset and spatial coverage of lake ice than when using a coarse dataset to initialize the lakes. While investigating the use of the one-dimensional lake model included with WRF (WRF-Lake), Xiao et al. (2016) noted that the use of these simplified lake models is limited due to the lack of horizontal mixing and ice movement, both of which are important for larger lake systems. Xue et al. (2017) used a two-way coupling of a climate model and FVCOM to show notable improvements over previous studies with simpler hydrodynamic components in terms of lake thermal properties and ice for simulations on climate time scales and mentions the importance of ice dynamics on shorter time scales.

While two-way coupling of atmospheric and hydrodynamic models has been shown to be successful for climate simulations, exchanging state variables or fluxes between the weather and ice-lake models at every time step is computationally expensive, especially for high-resolution models, such as HRRR and GLOFS. Timeliness is required for operational forecast models, and full model coupling would be too resource

intensive for the operational environment. On the other hand, coupling between the models via iterative one-way data sharing potentially provides a practical solution by allowing both the weather and ice-lake models to incorporate rapidly changing surface conditions. In the one-way linkage, the atmospheric model ingests the temporally changing forecasted lake-surface temperature and ice conditions (e.g., ice concentration, surface temperature) as the surface boundary conditions, instead of the conventional static lake-surface temperature from satellite-based analysis (sometimes out-of-date by several days from late fall to winter due to persistent cloud cover). In turn, the ice-hydrodynamic model (GLOFS) will receive “better” surface meteorology from the linked atmospheric model in the following forecast cycles. Thus, the one-way linkage approach enables loose iterative model coupling without increasing any computational expense by leveraging the existing dissemination channels for HRRR from NOAA’s National Weather Service (NWS) and for GLOFS from NOAA’s National Ocean Service (NOS).

The goal of this study is to evaluate the benefits of the one-way coupling between the atmospheric and ice-hydrodynamic models in simulating LES storms, particularly in simulating lake-surface conditions, turbulent heat fluxes over the lakes, and snow water equivalent (SWE) downwind of the lakes. We demonstrate that the one-way linkage between the weather and ice-lake models provides a practical approach to improving hazardous winter weather forecasts associated with LES events during periods of changing lake-surface conditions, including rapid ice cover evolution. Three case studies of LES events are presented along with verification of the one-way linkage approach. Model results are validated against available observations, including lake-surface temperature, turbulent heat fluxes from the lake surface, and SWE. The evidence provided in this study highlights the importance of coordinated improvements among different operational entities, such as NOS and NWS to provide more accurate forecasts at a relatively low computational cost.

In [section 2](#), we describe the atmospheric and ice-lake models used in our experiment, as well as the data used to validate the model results. In [section 3](#), we present the results from the numerical experiment and discuss how the models are improved by the one-way coupling and steps to further improve forecast accuracy. In [section 4](#), we summarize the study.

## 2. Methods

### *a. Atmospheric model*

The WRF-ARW Model ([Skamarock et al. 2008](#)), version 3.9.1 (hereafter WRF in this study), was used to simulate LES events over the Great Lakes region. The WRF offers rigorously tested numerical methods with capability for non-hydrostatic applications. The WRF configuration (including physics suite selection) was identical to the NOAA’s HRRR ([Benjamin et al. 2016a,b](#)), whose applications cover the entire contiguous United States and the Alaska region. However, our

application is to a restricted computational domain covering the Great Lakes region ([Fig. 1](#)) with a 3-km horizontal grid and 51 vertical hybrid-sigma levels. Key physics parameterizations include the Mellor–Yamada–Nakanishi–Niino (MYNN) ([Nakanishi and Niino 2004, 2009](#); [Olson et al. 2019](#)) planetary boundary layer schemes, the aerosol-aware microphysics of [Thompson and Eidhammer \(2014\)](#), and the Rapid Update Cycle (RUC) land surface model ([Smirnova et al. 2016](#)). The model is convection allowing and therefore no cumulus parameterization was used which is consistent with previous research using WRF at this horizontal grid spacing for this application (e.g., [Shi and Xue 2019](#); [Wright et al. 2013](#)). Hourly updated Rapid Refresh ([Benjamin et al. 2016a](#)) fields were used as initial and lateral boundary conditions as currently applied in operations. A one-dimensional lake model implemented in WRF ([Oleson et al. 2013](#)) was used for smaller inland lakes. Over the Great Lakes, the control lower boundary condition for the lake surface (i.e., lake-surface temperature) was prescribed using satellite-based observations based on the NOAA HIRES RTG 1/12th degree SST dataset ([https://polar.ncep.noaa.gov/sst/rtg\\_high\\_res/](https://polar.ncep.noaa.gov/sst/rtg_high_res/), hereafter referred to as RTG) at the model initialization and remains constant throughout the forecast period. For ice cover, the daily sea ice analysis from the NCEP was used ([Grumbine 2014](#)), which has 12.7-km horizontal resolution. Ice cover at a model pixel was handled as a binary value, that is, 100% (full coverage) or 0% (open water). These are based on the HRRR’s NOAA/NCEP operational version as of 2019. We define this quasi-operational setup with the WRF for the Great Lakes as the “control” case. In addition, we define the dynamic case as an experimental simulation where “dynamic” lake-surface conditions were provided by an ice-hydrodynamic model, FVCOM-CICE, which is described in the following section. In the dynamic case, the lake-surface conditions evolved over the simulation period with temporarily changing lake-surface temperature and fractional ice cover. Turbulent heat fluxes are calculated as a weighted average of over-water and over-ice values based on the areal fraction of ice provided by the ice-hydrodynamic model, FVCOM-CICE. To confirm the system convergence in the dynamic case, we conducted multiple iterations of data exchange between the WRF and FVCOM-CICE (see in the following section); the dynamic case returned its surface meteorology to force FVCOM-CICE, whose results were passed back to the WRF for the second iterative run. This process was repeated for three iterations, but the results in the WRF and FVCOM-CICE were found to essentially converge after the first iteration, which is further detailed in [section 3a](#).

The comparative study of the control and dynamic cases enable evaluations of improvements that the HRRR could merit by taking account of temporally evolving lake surface conditions and fractional ice cover in its future operational implementation. The simulations with the WRF were made for the durations of three selected LES events, which is listed in [Table 1](#) and further described in [section 2c](#).

### *b. Ice-hydrodynamic model*

The unstructured grid FVCOM ([Chen et al. 2006, 2013](#)) was used to simulate the Great Lakes hydrodynamics. FVCOM is a

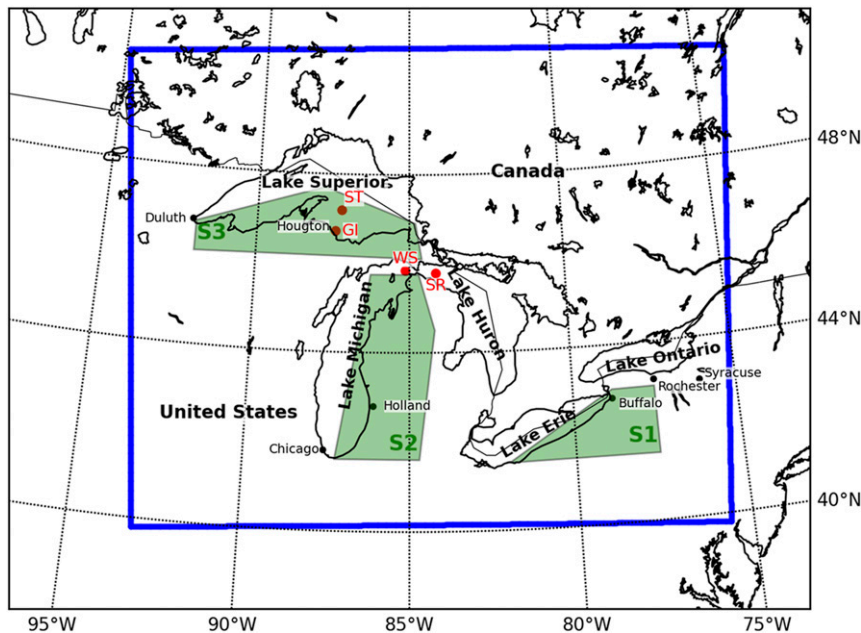


FIG. 1. Horizontal extent of domain used for the WRF simulations depicted by the blue box. Red dots represent flux-tower locations (ST: Stannard Rock, GI: Granite Island, WS: White Shoal, SR: Spectacle Reef). Polygons shown in green are the downwind areas where the threat score of snow water equivalent simulations was evaluated (S1: Erie, S2: Michigan, and S3: Upper Peninsula).

three-dimensional, free-surface, primitive equation, sigma-coordinate oceanographic model that solves the integral form of the governing equations. FVCOM has been applied in several studies of the coastal ocean, including successful application to the Great Lakes (Anderson et al. 2010; Anderson and Schwab 2012, 2013; Anderson et al. 2015; Bai et al. 2013; Xue et al. 2015; and many others). In this work, the model was configured separately for Lake Superior, Lake Erie, and Lake

Ontario, while Lake Michigan and Lake Huron, which are connected by the Strait of Mackinac and form a single system, are handled by the same model. Horizontal grid resolution in each configured model ranged from roughly 200 m near the shoreline to 2500 m offshore, with 21 vertical sigma layers evenly distributed throughout the water column. As a result, the numbers of triangular elements in the models are roughly 20 000 for Lake Superior, 170 000 for Lake

TABLE 1. Lake-effect snow events focused on in the model study. The cooling values ( $^{\circ}\text{C}$ ) are from the satellite analysis (RTG), and the values per day are shown in the parentheses. The gained ice coverage values (%) are from the NIC analysis. Both the cooling and gained ice coverage are for the storm durations.

Event name	Duration	Impacted area	Cooling of lake surface temperature ( $^{\circ}\text{C}$ )	Gained ice coverage (%)
Nov 2014	0000 UTC 17 Nov–1800 UTC 19 Nov 2014	Downwind Lake Erie	Superior: 0.45 (0.16) Michigan: 1.18 (0.43) Huron: 1.32 (0.48) Erie: 1.52 (0.55) Ontario: 1.15 (0.42)	Ice-free
Dec 2017	1200 UTC 24 Dec–0000 UTC 27 Dec 2017	Downwind Lake Erie, Upper Peninsula of Michigan	Superior: 0.80 (0.32) Michigan: 1.25 (0.50) Huron: 0.95 (0.38) Erie: 1.45 (0.58) Ontario: 0.15 (0.06)	Superior: 3 Michigan: 3 Huron: 9 Erie: 9 Ontario: 1
Jan 2018	0000 UTC 3 Jan–0300 UTC 6 Jan 2018	Downwind Lake Michigan, Upper Peninsula of Michigan	Superior: 1.05 (0.34) Michigan: 0.77 (0.25) Huron: 0.57 (0.18) Erie: 0.70 (0.22) Ontario: 0.03 (0.01)	Superior: 3 Michigan: 9 Huron: 6 Erie: 40 Ontario: 9



Michigan–Huron, 12 000 for Lake Erie, and 100 000 for Lake Ontario. For the Lake Erie and Lake Michigan–Huron models, these implementations of FVCOM are based on the next-generation of NOAA’s GLOFS (Anderson et al. 2018), while they are experimental for the Lake Superior and Lake Ontario models. Horizontal and vertical diffusion are handled by the Smagorinsky parameterization (Smagorinsky 1963) and Mellor–Yamada level-2.5 turbulence closure scheme (Mellor and Yamada 1982; Mellor and Blumberg 2004), respectively. The air–water drag coefficient was calculated as a function of wind speed (Large and Pond 1981). Latent and sensible heat fluxes were calculated from the Coupled Ocean–Atmosphere Response Experiment (COARE; Fairall et al. 1996a,b, 2003) algorithm. Modeled depths were taken from 3-arc-second bathymetry data from the NOAA National Centers for Environmental Information (NCEI; Fig. S1 in the online supplemental material).

UG-CICE (Gao et al. 2011; Hunke et al. 2015) has been included and coupled within FVCOM. The UG-CICE model includes components for ice thermodynamics and ice dynamics, using elastic-viscous-plastic rheology for internal stress (Hunke and Dukowicz 1997), and produces two-dimensional fields of ice concentration, thickness, and velocity. A multi-category ice thickness distribution (ITD) model (Thorndike et al. 1975) is employed in UG-CICE to represent the subgrid scale distribution of ice thickness in response to mechanical and thermal forcing. Hereafter, we call the coupled FVCOM and UG-CICE system as FVCOM-CICE. In this study, five categories of ice thickness were defined (5, 25, 65, 125, and 205 cm). The modeled ice surface albedo depends on surface temperature and thickness of ice, as well as the visible and infrared spectral bands of the incoming solar radiation (Briegleb 1992). At ice-covered cells, the net momentum transfer was calculated as a weighted average of the air–water and ice–water stresses by areal fraction of ice. The air–ice drag coefficient  $C_{D,ai}$  was calculated as a function of wind speed  $U$ , given as  $C_{D,ai} = (1.43 + 0.052U) \times 10^{-3}$  and the ice–water drag coefficient is  $5.5 \times 10^{-3}$ . Similarly, the net heat transfer was calculated as a weighted average of the air–water and ice–water heat fluxes. The ice–water heat fluxes are calculated based on the bulk transfer formula (Maykut and McPhee 1995).

The background FVCOM-CICE simulations were started at least one year prior to each of the selected LES events (Table 1) to obtain the realistic thermal structures. These background simulations were forced by the hourly meteorological datasets from HRRR. Seasonal evolutions of water temperature and ice coverage with similar FVCOM-CICE setups were extensively verified in Anderson et al. (2018) and Fujisaki-Manome et al. (2020). For the one-way coupling experiments, the models started in the beginning of the LES events using restart files from the background simulations. In these experiments, the models were forced by the 15-min meteorological datasets from WRF (section 2a). To assess the impact of temporally evolving lake surface conditions in WRF simulations, the lake-surface temperature was debiased to match its lake-wide mean to RTG’s. For the iterative runs of the one-way coupling mentioned in section 2a, FVCOM-CICE was forced by the control case of WRF in the first iteration and

passed its resulting lake surface conditions to WRF for its first iteration (i.e., the dynamic case). The second iteration of FVCOM-CICE was forced by the dynamic case of WRF.

### c. Lake-effect snow events

The three LES events presented (Table 1) were selected to test the modeling framework in specific ways. The first two cases (November 2014 and December 2017) were high-impact events with large snowfall accumulations. The November 2014 event was a result of an anomalously cold-air outbreak early in the unstable season, when the lake-surface forcing potential was very high. Resultant lake-effect convection produced over 5 feet ( $\sim 1.5$  m) of snowfall during an approximate 48-h period across areas downwind of Lake Erie (NWS 2014). Based on the satellite-based analysis from RTG, the daily cooling of the mean lake surface temperatures (Table 1) well exceeded the climatological upper bound ( $0.21^{\circ}\text{C day}^{-1}$  based on Fichot et al. 2019, see section 1) in Lake Michigan ( $0.43^{\circ}\text{C day}^{-1}$ ), Lake Huron ( $0.48^{\circ}\text{C day}^{-1}$ ), Lake Erie ( $0.55^{\circ}\text{C day}^{-1}$ ), and Lake Ontario ( $0.42^{\circ}\text{C day}^{-1}$ ), but not in Lake Superior ( $0.16^{\circ}\text{C day}^{-1}$ , Table 1). The lakes were ice-free during this event. The December 2017 event produced a record 24-h snowfall at Erie International Airport in Pennsylvania of over 30 in. ( $\sim 0.75$  m), while also dropping heavy snowfall over Michigan’s Upper Peninsula and western New York (NWS 2017, 2018). The daily cooling of the mean lake surface temperatures (Table 1) again well exceeded the climatological upper bound in Lake Superior ( $0.32^{\circ}\text{C day}^{-1}$ ), Lake Michigan ( $0.50^{\circ}\text{C day}^{-1}$ ), Lake Huron ( $0.38^{\circ}\text{C day}^{-1}$ ), and Lake Erie ( $0.58^{\circ}\text{C day}^{-1}$ ), but not in Lake Ontario ( $0.06^{\circ}\text{C day}^{-1}$ ). The lakes were largely ice free but in Lake Huron and Lake Erie, ice coverage over each of the two lakes increased by 9% during the storm duration (Table 1). These two events were characterized by rapidly changing lake-surface temperatures and are well suited to test the modeling framework’s ability to resolve and potentially improve strongly forced, high-impact events using updated lake-surface conditions. The final case study (January 2018) occurred during the same cold-air outbreak as the December 2017 event. This event resulted in lake-effect snowfall downwind of all the Great Lakes along with rapidly growing ice coverage over the lakes. This event occurred after the fall overturn and the cooling of lake-surface temperatures was not as evident as the other two events. However, the daily cooling of the mean lake surface temperatures (Table 1) were still above or around the climatological upper bounds in Lake Superior ( $0.34^{\circ}\text{C day}^{-1}$ ), Lake Michigan ( $0.25^{\circ}\text{C day}^{-1}$ ), and Lake Erie ( $0.22^{\circ}\text{C day}^{-1}$ ). There were notable growths of ice cover during the 3-day event, particularly in Lake Erie, which gained 40% ice cover during the storm duration. This case was well posed to test the modeling framework in rapidly changing lake-surface conditions, which were not captured in previous modeling configurations that use static lake-surface conditions.

### d. Data for model verification

#### 1) SURFACE METEOROLOGY

Simulated wind speed and air temperature from the atmospheric model were compared with observations from the National

Data Buoy Center's Coastal Marine Automated Network (CMAN), whose data were obtained from the NOAA Great Lakes CoastWatch website (<https://coastwatch.glerl.noaa.gov/marobs/>). Modeled ice concentration and spatial distribution simulated by FVCOM were compared to Great Lakes ice concentration data from the U.S. National Ice Center (NIC; [https://www.natice.noaa.gov/products/great\\_lakes.html](https://www.natice.noaa.gov/products/great_lakes.html)). Through a binational coordinated effort between the U.S. NIC and Canadian Ice Center, routine gridded ice analysis products are produced from available data sources including *RadarSat-2*, *Envisat*, the Advanced Very High Resolution Radiometer (AVHRR), Geostationary Operational and Environmental Satellites (GOES), and Moderate Resolution Imaging Spectroradiometer (MODIS). To compare with a spatial pattern of water surface temperature from the FVCOM simulations, the Great Lakes Surface Environmental Analysis (GLSEA; Schwab et al. 1999; <https://coastwatch.glerl.noaa.gov/glsea/doc/>) was used. GLSEA provides daily water surface temperature for the Great Lakes at ~1.3-km resolution from the composite analysis of NOAA's AVHRR imagery. Because a temporal smoothing over  $\pm 10$  days is applied to GLSEA, the product is not ideal to look at short-term changes over a few days; however, we took advantage of its high-resolution spatial pattern by verifying the overall spatial pattern of the FVCOM-simulated water surface temperature on the initial time of each simulation. The RTG dataset was used for the verification of the changes in lake-wide mean water surface temperature during the events.

## 2) TURBULENT HEAT FLUXES

Turbulent heat flux data from four offshore platforms were used to compare with the simulated turbulent sensible and latent heat fluxes ( $\lambda E$  and  $H$ , respectively) by WRF. The data were collected from offshore, lighthouse-based monitoring platforms (Fig. 1): Stannard Rock (Lake Superior), Granite Island (Lake Superior), White Shoal (Lake Michigan), and Spectacle Reef (Lake Huron). These observations are part of a broader collection of fixed and mobile-based platforms collectively referred to as the Great Lakes Evaporation Network (GLEN; Lenters et al. 2013; Spence et al. 2011; Blanken et al. 2011). Some of these installations are referred by NDBC as stations STDM4, WSLM4, and SRLM4 at Stannard Rock, White Shoal, and Spectacle Reef, respectively. All eddy covariance systems followed conventional protocols for calculating turbulent fluxes, such as those established in the Great Slave Lake (Northwest Territories, Canada) by Blanken et al. (2000). Mean turbulent fluxes over 30-min increments were provided for latent and sensible heat.

## 3) SNOW WATER EQUIVALENT

The Snow Data Assimilation System (SNODAS) is a modeling and data assimilation system developed by the NOAA/NWS's National Operational Hydrologic Remote Sensing Center (NOHRSC) to provide the best possible estimates of snow cover and associated variables as gridded data to support hydrologic modeling and analysis (Barrett 2003). Here, the data were considered as an observational

analysis to compare with simulated SWE from the atmospheric model. The domain covers the contiguous United States, and the data are provided daily with a 1-km horizontal resolution.

## e. Skill assessment

To assess the modeled lake-surface conditions, turbulent heat fluxes, and snow water equivalent, a few metrics are introduced. First, changes in lake-surface conditions (i.e., lake-surface temperature, ice coverage) during an LES event ( $\Delta X$ ) were calculated as

$$\Delta X = X_{t=t_{\text{end}}} - X_{t=t_{\text{start}}}, \quad (1)$$

where  $X_{t=t_{\text{end}}}$  and  $X_{t=t_{\text{start}}}$  are values of lake-wide mean water surface temperature or ice coverage at the end and start times of an LES event, respectively.

Second, the root-mean-square error (RMSE) was used to evaluate the modeled surface meteorology and the turbulent heat fluxes:

$$\text{RMSE} = \left[ \frac{1}{N} \sum_{i=1}^N (x_m - x_o)^2 \right]^{1/2}, \quad (2)$$

where  $N$  is the number of data points and  $x_m$  and  $x_o$  are modeled and observed values, respectively.

Third, to evaluate a modeled spatial pattern of snow water equivalent, the mean absolute error (MAE) difference was used. The MAE difference, noted as  $\Delta \text{MAE}$ , was calculated as

$$\Delta \text{MAE} = |\text{SWE}_m^d - \text{SWE}_o| - |\text{SWE}_m^c - \text{SWE}_o|, \quad (3)$$

where  $\text{SWE}_m^d$  and  $\text{SWE}_m^c$  are modeled snow water equivalent in the dynamic and control cases, respectively.  $\text{SWE}_o$  is the snow water equivalent from SNODAS. Given that the sign of bias (i.e.,  $|\text{SWE}_m^c - \text{SWE}_o|$ ) rarely changed in the control and dynamic cases (as detailed in section 3c), negative  $\Delta \text{MAE}$  indicates improvement in the dynamic case against the control case (due to reduction in MAE) and positive  $\Delta \text{MAE}$  indicates degradation (due to increase in MAE).

Last, to quantify the model's skill in simulating SWE, the threat score (TS) was used. TS is often used when evaluating a model's categorical forecast skill such as to capture observed "yes" (e.g., occurrence of a certain amount of snowfall) events and can be calculated as below:

$$\text{TS} = N_h / (N_h + N_m + N_f), \quad (4)$$

where  $N_h$ ,  $N_m$ , and  $N_f$  are the numbers of hit, miss, and false alarm pixels, respectively. Note that the number of correct negative (e.g., success in simulating no snowfall occurrence) is not included in the above equation. A forecast or model "yes" pixel was defined based on three thresholds for the increase in SWE during a simulation period ( $\Delta \text{SWE}$ ), that is, when  $\Delta \text{SWE}$  exceeded 10, 20, and 30 kg m<sup>-2</sup>, respectively, a pixel is assigned with "yes" for corresponding thresholds, otherwise "no". These thresholds were based on the range of the SNODAS analysis over the Great Lakes. After the SNODAS analysis was interpolated to the WRF model grid, "yes" or "no" was

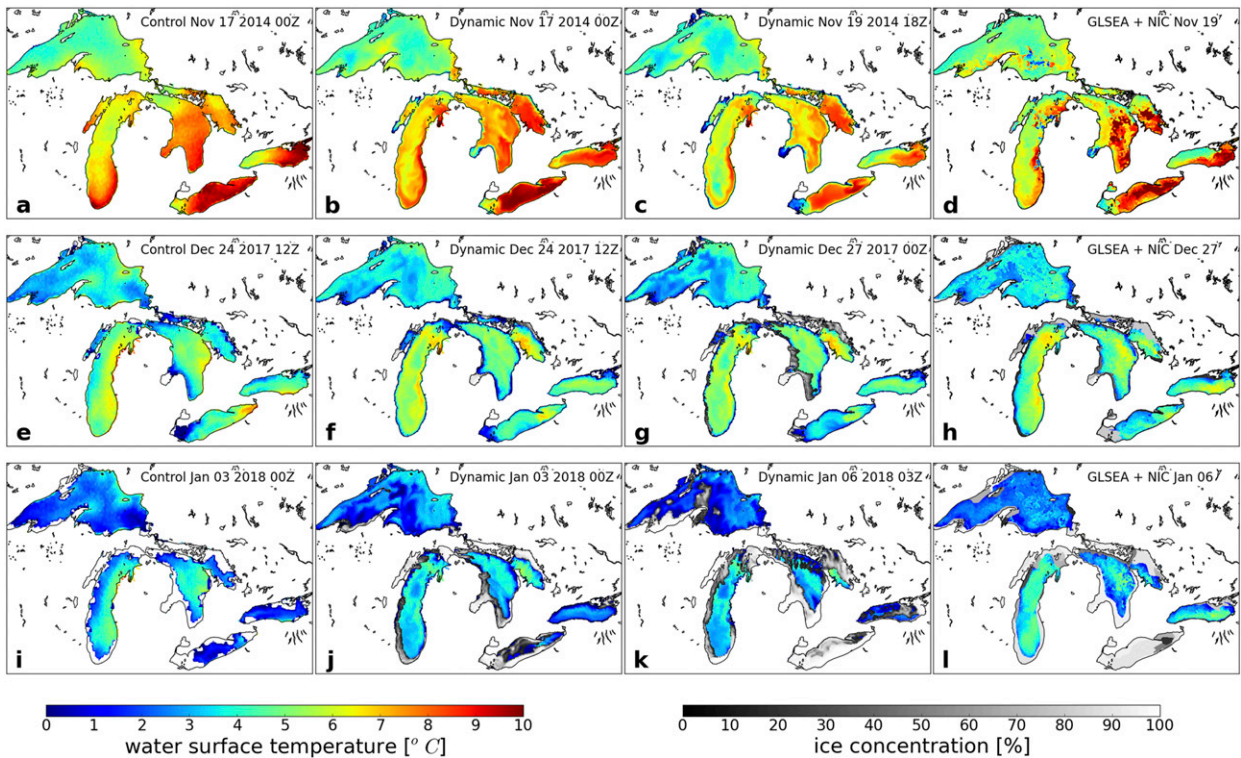


FIG. 2. Water surface temperature and lake ice cover for the three lake-effect snow events. From left to right, columns show (a),(e),(i) the control case; (b),(f),(j) the dynamic case at the initial simulation times; (c),(g),(k) the dynamic case at the end simulation times; (d),(h),(l) and analyses from GLSEA and NIC on the end days of simulations. From top to bottom, rows show (a)–(d) the November 2014 event, (e)–(h) the December 2017 event, and (i)–(l) the January 2018 event.

assigned to each pixel for the three intensity levels both in the model results and the interpolated SNODAS analysis. The number of hits  $N_h$  was obtained by counting pixels where both the model results and interpolated SNODAS analysis had “yes.” The number of misses  $N_m$  (false alarms  $N_f$ ) was calculated by counting pixels where the interpolated SNODAS analysis had “yes” (“no”) but the model results had “no” (“yes”).

### 3. Results and discussions

#### a. Lake-surface conditions

Figure 2 shows the water surface temperature and ice cover at initial and end simulation times. At the initial time, the control simulation (Figs. 2a,e,i) had similar water surface temperature to the dynamic simulation (Figs. 2b,f,j) for all three events. However, the control lacked the detailed spatial representations, such as nearshore–offshore gradients in Lake Michigan and cooling in Saginaw Bay which is located in the southwest corner of Lake Huron (Figs. 2a,b). These detailed features were captured within the dynamic simulation. The contrast of binary and fractional ice covers in the control and dynamic cases should be also noted in the January 2018 event (Figs. 2i,j). Over the simulation periods, FVCOM-CICE reproduced the dynamic change of the lake-surface conditions in response to exposure to the cold air mass. The modeled water

surface temperature and ice cover at the end times (Figs. 2c,g,k) were in reasonable agreement with the analyses from GLSEA and NIC (Figs. 2d,h,i). Furthermore, for all simulations, the final lake-surface temperature was notably cooler than the initial state. In the December 2017 and January 2018 events, the dynamic simulations capture notable development of ice cover on Lake Erie (Figs. 2h,j and 3). On the other hand, the control lake-surface condition remained constant, missing the rapid ice development. It is also notable that most of the ice areas in the dynamic simulation were fractional in nature (i.e., less than 100%), while in the control case, ice cover was handled as a binary condition (i.e., 0% or 100%). The rapid cooling of the lake surfaces was clearly demonstrated by the time trends of lake-wide mean temperatures (Fig. 4), where notable decreases of lake-wide mean temperature were captured by the FVCOM-CICE simulation results and were in agreement with the analyses. Most notably, Lake Erie experienced the greatest cooling among the lakes, with  $\Delta T_{\text{FVCOM}}$  ranging from  $-0.28^\circ$  to  $-1.78^\circ\text{C}$  ( $\Delta T_{\text{RTG}}$  ranging from  $-0.7^\circ$  to  $-1.52^\circ\text{C}$ ) during the storm events. This can be attributed to Lake Erie being the shallowest among the Great Lakes and therefore has the lowest heat capacity. These rapid surface condition changes demonstrate the shortfall of using a temporally static surface boundary condition, which does not take into account the cooling lake-surface temperatures leading to errors in lake-surface temperature by the end of the simulation on the order



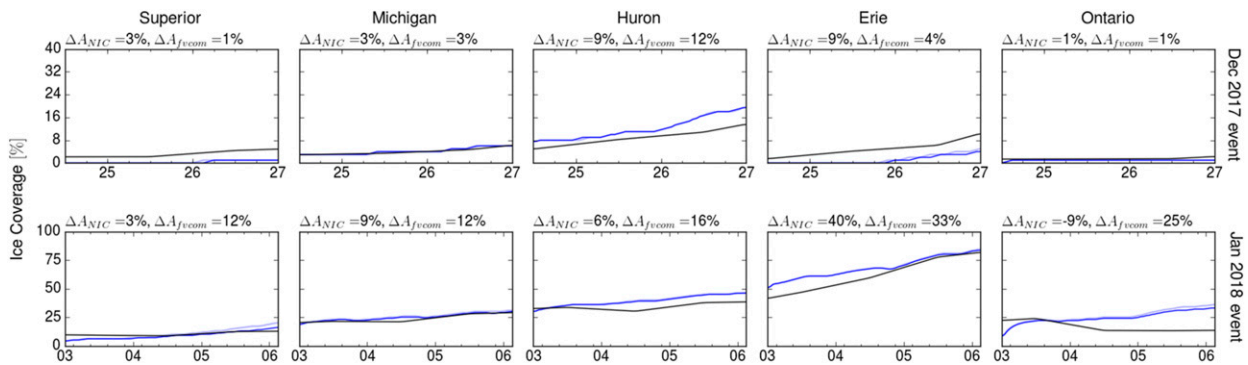


FIG. 3. Lake-wide ice coverage for each of the Great Lakes during (top) the December 2017 and (bottom) the January 2018 events. There was no ice during the November 2014 event. Thick and thin blue lines denote the FVCOM-CICE simulation results after the first and second iterations, respectively. Black lines show the analyses from NIC. On top of each panel, the change in ice coverage (%) during each event for each lake is shown for the NIC analysis ( $\Delta A_{NIC}$ ) and the FVCOM simulation ( $\Delta A_{FVCOM}$ ).

of  $1^{\circ}\text{C}$  over many of the lakes. Solution convergence was tested via additional iterations of the loosely coupled modeling system. The net result with both lake-wide ice coverage and water surface temperature was only minimal changes from the first loosely coupled solution.

Figure 5 shows wind at 10 m and air temperature at 2 m above the surface for the control and dynamic simulations. Changes in wind were limited to minor circulation changes associated with altered lake-effect band locations. For 2-m air temperature, both the control (Figs. 5b,f,j) and dynamic (Figs. 5c,g,k) solutions successfully handled the notable cooling over the computational domain through the simulation periods. For the November 2014 event, the dynamic solution was cooler than the control over the lakes at the end of simulation (Fig. 5d). This is an expected result, as the dynamic simulation incorporated the cooling lake surface. In contrast, the

December 2017 and January 2018 events had the opposite result (i.e., the control results had lower 2 m air temperature over the lakes at the end of simulation compared to the dynamic results). The cooler air in the control results was most notable over ice cover (Fig. 2) and had a strong influence on lake average values. Recall the default behavior of the control simulation is to assign lake ice coverage to 100% (no lead or fractional open water) for grid points assigned to ice. This treatment results in an overly cooled lake surface in the simulations where newly forming ice occurs, as in reality, there is exposure of water surface to the air due to fractional ice cover and/or leads. In the dynamic simulations, some of the exposure to open water is accounted for with the introduction of fractional ice cover.

To verify the modeled surface meteorology, the surface air temperature and wind speed from the case studies were

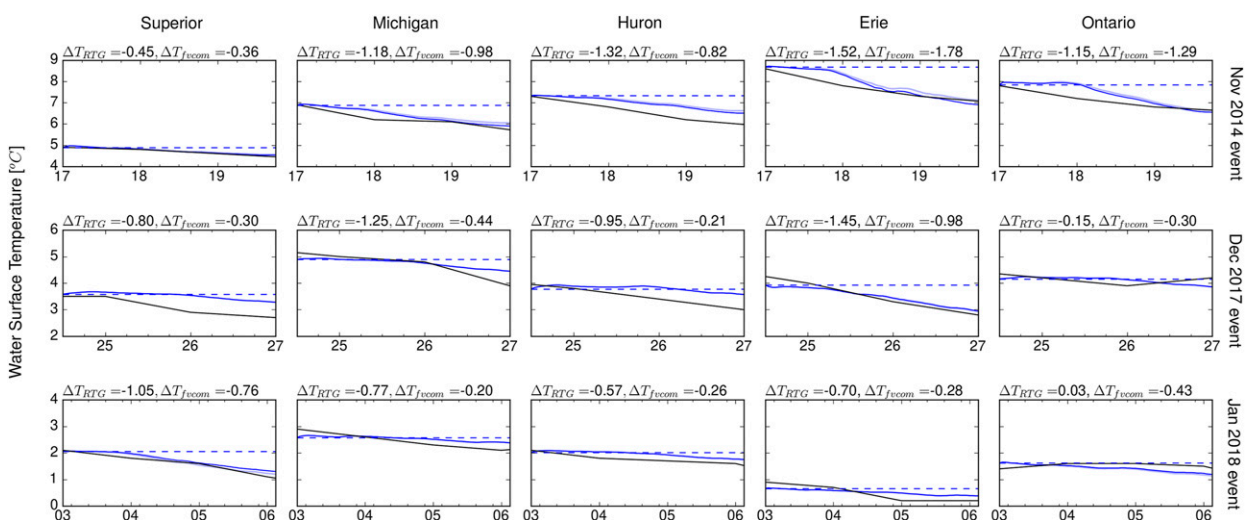


FIG. 4. Lake-wide mean temperature for each of the Great Lakes. Blue dashed lines denote the control case; thick and thin solid blue lines denote the FVCOM-CICE simulation results after the first and second iterations, respectively. Black lines show the analyses from RTG. From top to bottom, the rows indicate the November 2014 event, the December 2017 event, and the January 2018 event. On top of each panel, the temperature change during each event for each lake is shown for the RTG ( $\Delta T_{RTG}$ ) and the FVCOM simulation ( $\Delta T_{FVCOM}$ ).



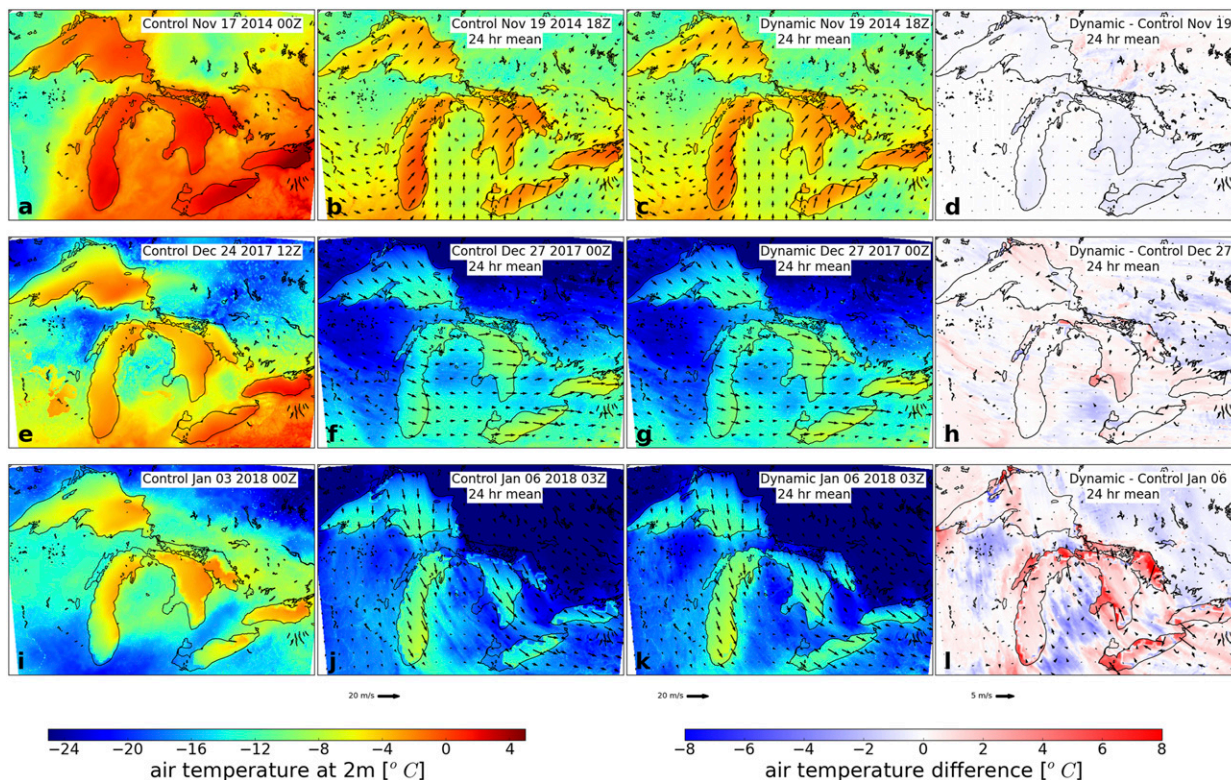


FIG. 5. Air temperature at 2 m from the surface (color) and wind vector at 10 m from the surface. Columns from left to right: (a),(e),(i) the control case at the initial time; (b),(f),(j) the last 24 h mean of the control case; (c),(g),(k) the last 24 h mean of the dynamic case; and (d),(h),(l) difference between the control and dynamic case over the last 24 h. Rows from top to bottom: (a)–(d) the November 2014 event (now missing), (e)–(h) the December 2017 event, and (i)–(l) the January 2018 event.

compared with the 15 coastal stations across the Great Lakes from CMAN (Figs. S1–S5). The RMSEs and biases were reduced at more than half of these stations using the dynamic configuration (Tables S1–S3). The improvements were most notable in the January 2018 event, likely due to not only the temporary evolving surface ice and water temperature conditions simulated by FVCOM-CICE, but also the improved ice treatment in the WRF (i.e., fractional ice).

*b. Turbulent heat fluxes*

Figure 6 shows the time series of lake-wide means of turbulent sensible and latent heat fluxes ( $H_s$  and  $H_l$ ). All the events exhibited notable peaks in these heat fluxes during the event periods, which were associated with the large temperature and humidity differences between the air and lake surface. Overall, the  $H_s$  (red lines in Fig. 6) were dominant compared with the  $H_l$  (blue lines in Fig. 6). The comparison with the observations at the GLEN sites is also shown in Figs. 7 and 8. While comparisons to a very limited dataset like GLEN should be interpreted with caution, it is useful using higher-order data to offer insights to capabilities of the system in generating the appropriate atmospheric adjustment for these strong forcing scenarios.

For the November 2014 event, the difference in the lake-wide average  $H_s$  and  $H_l$  was relatively small between the

control and dynamic results (the first row in Fig. 6), with dynamic being slightly lower. This is consistent with the lake-surface cooling captured by the dynamic setup resulting in decreased air–lake temperature differences, thereby reducing turbulent heat fluxes. In comparison with the GLEN observations, the  $H_s$  simulation was improved at all the sites using the dynamic configuration (Fig. 7). The  $H_l$  simulation had mixed signals at these limited data points. Improvement was notable at Spectacle Reef, but degradation in performance occurred at Stannard Rock (Fig. 8).

For the December 2017 event, the lake-wide mean  $H_s$  and  $H_l$  from the two simulations were nearly identical. Unlike the November 2014 event, the cooling of lake surface was far less pronounced (Fig. 4), as temperatures were much closer to 0°C with notable ice development (Fig. 3). The only exception was Lake Huron, where  $H_s$  and  $H_l$  were notably higher in the dynamic results. During this event, Lake Huron was covered by 10%–20% of lake ice, while the other lakes were nearly ice-free (Fig. 3). As noted earlier, the control setup tended to produce a colder lake surface due to the binary treatment of ice cover, which was improved in the dynamic representation using fractional ice cover. The net result was slightly higher  $H_s$  and  $H_l$  across Lake Huron in the dynamic treatment. In general, the RMSE values using GLEN observations were similar between the control and dynamic simulations. However, near

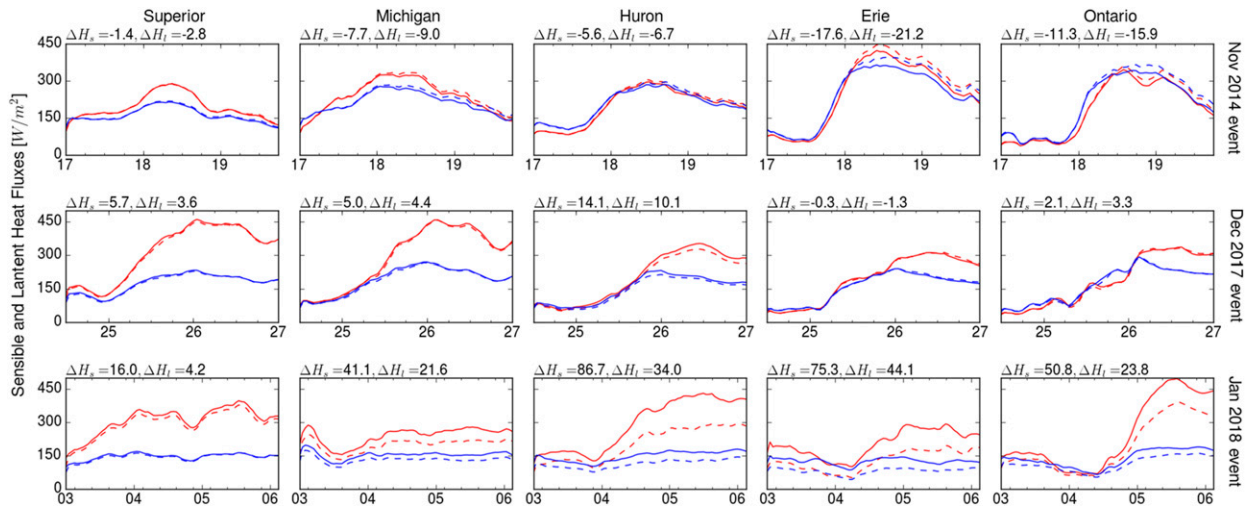


FIG. 6. Lake-wide averages of the turbulent sensible (red lines) and latent (blue lines) heat fluxes for the four events. From top to bottom, the rows show the November 2014 event, the December 2017 event, and the January 2018 event. Dashed line denotes the control case and solid line denotes the dynamic case.

the Straits of Mackinac, where notable ice cover was present, the RMSE for  $H_l$  was notably reduced at Spectacle Reef in the dynamic outcome (Fig. 8).

For the January 2018 event, the difference between the two simulations was the most prominent among the three cases. Overall, the dynamic simulation produced higher  $H_s$  and  $H_l$  than the control (Fig. 6). This was due to the notable area of fractional (not full) ice cover on most of the lakes. The control produced appreciably lower surface temperatures—especially where full, nonfractional ice cover was prescribed. This signal was more pronounced in the turbulent sensible heat flux  $H_s$ , as the dynamic simulation fractional ice cover allowed for a warmer lake surface (i.e., combination of ice and water). A comparative increase in the turbulent latent heat flux  $H_l$  is also noted in the dynamic simulation, except for over Lake Superior. It was slightly counterintuitive that the lake-wide mean  $H_s$  and  $H_l$  were smaller in the control case where ice coverage did not increase than those in the dynamic case where ice coverage increased in time, in the light of the conventional notion that growing ice cover on a lake insulates the lake and reduces the turbulent heat flux across the air and lake (Gerbush et al. 2008). This process certainly occurred in the dynamic case, but apparently, the inclusion of fractional ice cover had larger impacts on the experiment results. The RMSEs for  $H_s$  and  $H_l$  were mostly decreased in the dynamic case (Figs. 7 and 8), except for the turbulent sensible heat flux  $H_s$  at White Shoal, where the dynamic case overestimated the observed  $H_s$  value. The representation of fractional ice cover at White Shoal was consistent with NIC: the dynamic case had ice coverage of 90%–100% at the site, while NIC showed 90%–95%. One possible explanation is that the footprint of the eddy covariance measurement (which is often smaller than horizontal resolutions in FVCOM-CICE and NIC) was dominated by ice cover and therefore did not catch the signal from leads (i.e., small fraction of open water). In the control case, by definition, ice cover was assumed to be 100% (full).

### c. Snow water equivalent

Increase of snow water equivalent ( $\Delta$ SWE) during each LES event was reasonably captured by the modeling system in comparison with the SNODAS analysis (Figs. 9a–i). As expected, the largest accumulation of SWE was concentrated in the three downwind areas of the lakes defined in Fig. 1. At first glance, the spatial patterns of  $\Delta$ SWE were similar between the control and dynamic results (i.e., the second and third rows in Fig. 9). However, the difference plots (Figs. 9j–l) show evident changes in the downwind areas. The spatial patterns of differences were a mixture of positive and negative changes, and so were the MAE differences ( $\Delta$ MAE, Figs. 9m–o). Overall, the differences (Figs. 9j–l) appear to reflect the changes in the turbulent heat fluxes  $H_s$  and  $H_l$  from the lakes (Fig. 6). For example, in the November 2014 event, the dynamic simulation produced less  $\Delta$ SWE (i.e., more blue areas in Fig. 9j) downwind of most of the lakes compared to the control as a result of the reduced  $H_s$  and  $H_l$  from the lakes. Similarly, in the January 2018 event, the dynamic results generally higher than the control (positive  $\Delta$ SWE—i.e., more red areas in Fig. 9l) as a result of the increased  $H_s$  and  $H_l$  from the lakes.

At a subbasin scale, there were a few notable improvements. For example, in the November 2014 event, the overspread of  $\Delta$ SWE in the south of Lake Erie within the control outcomes were reduced within the dynamic simulation (blue area in Fig. 9m). Notable reduction of MAE was also seen downwind of southern Lake Michigan in the December 2017 event (Fig. 9n), and again downwind of Lake Erie in the January 2018 event (Fig. 9o). On the other hand, there are issues that neither of the model experiments were able to address, such as the deep overspread of  $\Delta$ SWE across the inland regions of lower Michigan in the December 2017 event (Figs. 9k,n) and the overestimate of  $\Delta$ SWE downwind of northern Lake Michigan (Figs. 9l,o) in the January 2018 event.

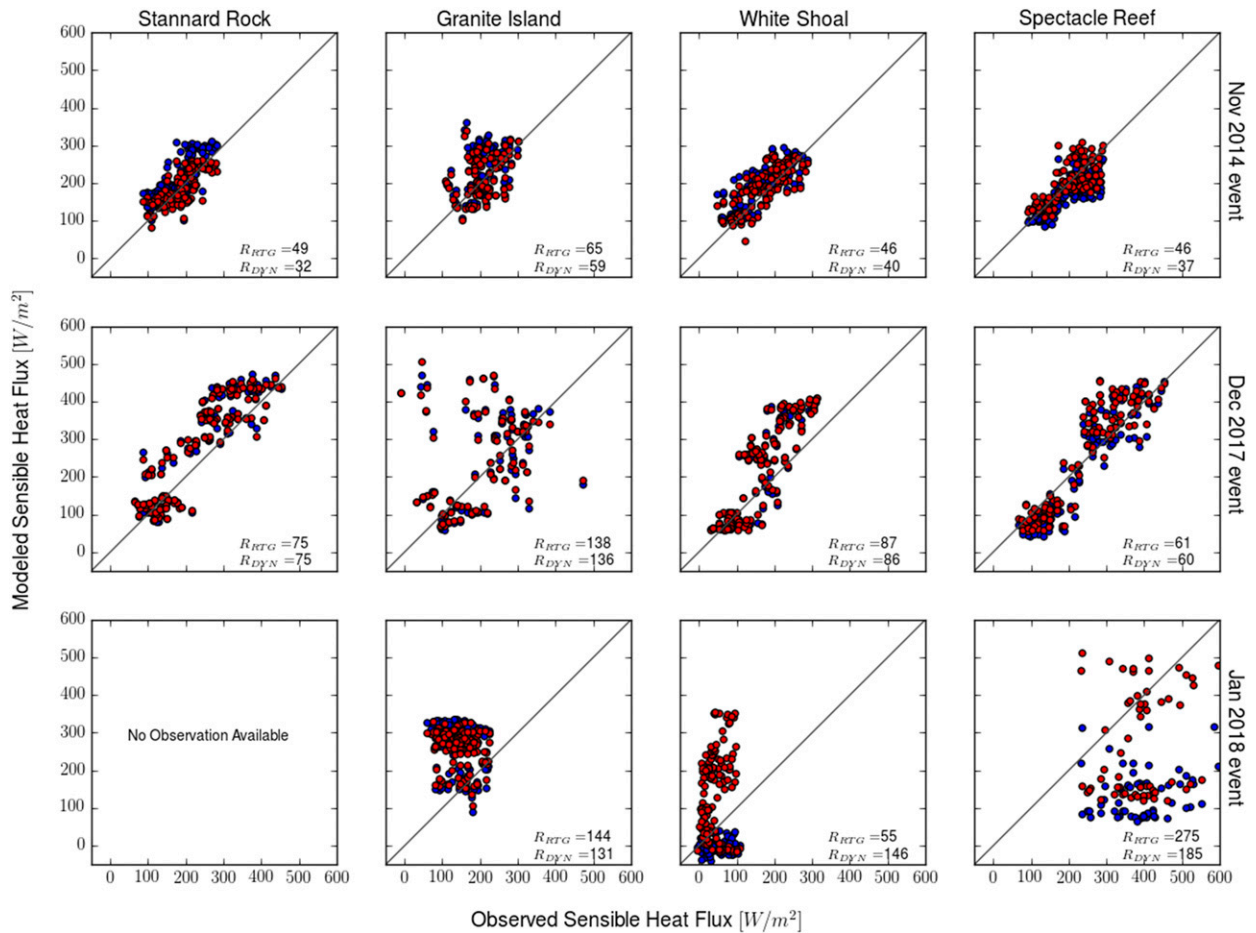


FIG. 7. Comparison of the modeled and observed turbulent sensible heat flux  $H_s$  during the three events. The observations are from the GLEN sites of Stannard Rock (Lake Superior), Granite Island (Lake Superior), White Shoal (Lake Michigan), and Spectacle Reef (Lake Huron). The model results are taken from the closest grid points to the observation sites. Blue and red dots indicate the results from the control and dynamic cases, respectively. RMSE values ( $W m^{-2}$ ) for the control and dynamic cases ( $R_{RTG}$  and  $R_{DYN}$ ) are shown on the lower right of each panel.

The threat scores across the three downwind regions are shown in Table 2. The most evident improvement was seen with the January 2018 event, where the score was notably improved downwind of Lake Erie and Lake Michigan. Across the Upper Peninsula (UP) of Michigan, the score remained almost the same for this event. For the November 2014 and December 2017 events, the scores were a mixture of slight improvements, degradation, and no change. On average, the score was improved for all the thresholds in the dynamic results. The largest improvement in the January 2018 event was likely associated with the notable coverage of lake ice during this event and its improved treatment in the dynamic setup (i.e., fractional ice coverage).

*d. Operational applicability*

The verification presented in the previous subsections demonstrates that the one-way linkage between FVCOM-CICE and WRF resulted in improved simulation performance of surface meteorology and  $\Delta SWE$  during the selected LES

events. The realistic representation and frequent updates of lake ice coverage and water surface temperature clearly propagated into the improved simulations of the turbulent heat fluxes and snow water equivalent in the downwind areas.

LES events generally involve notable change in the lake-surface conditions (i.e., temperature, ice cover) over a few-day period. Thus, the advantage of the one-way linkage was well illustrated in these case studies. Even in other seasons, benefits of the one-way linkage can be expected. For example, coastal upwelling is a typical nearshore event in the Great Lakes during summer [e.g., Lake Erie (Rowe et al. 2019) and Lake Michigan (Plattner et al. 2006)] and is associated with a subdaily change in lake-surface temperature and sharp nearshore-offshore temperature gradient. Such features are often missed in the daily  $1/4^\circ$  resolution RTG product but can be captured by FVCOM-CICE.

The one-way linkage procedure was iterated over for multiple times in a preliminary experiment. From those experiments, it was found that the model setup results mostly



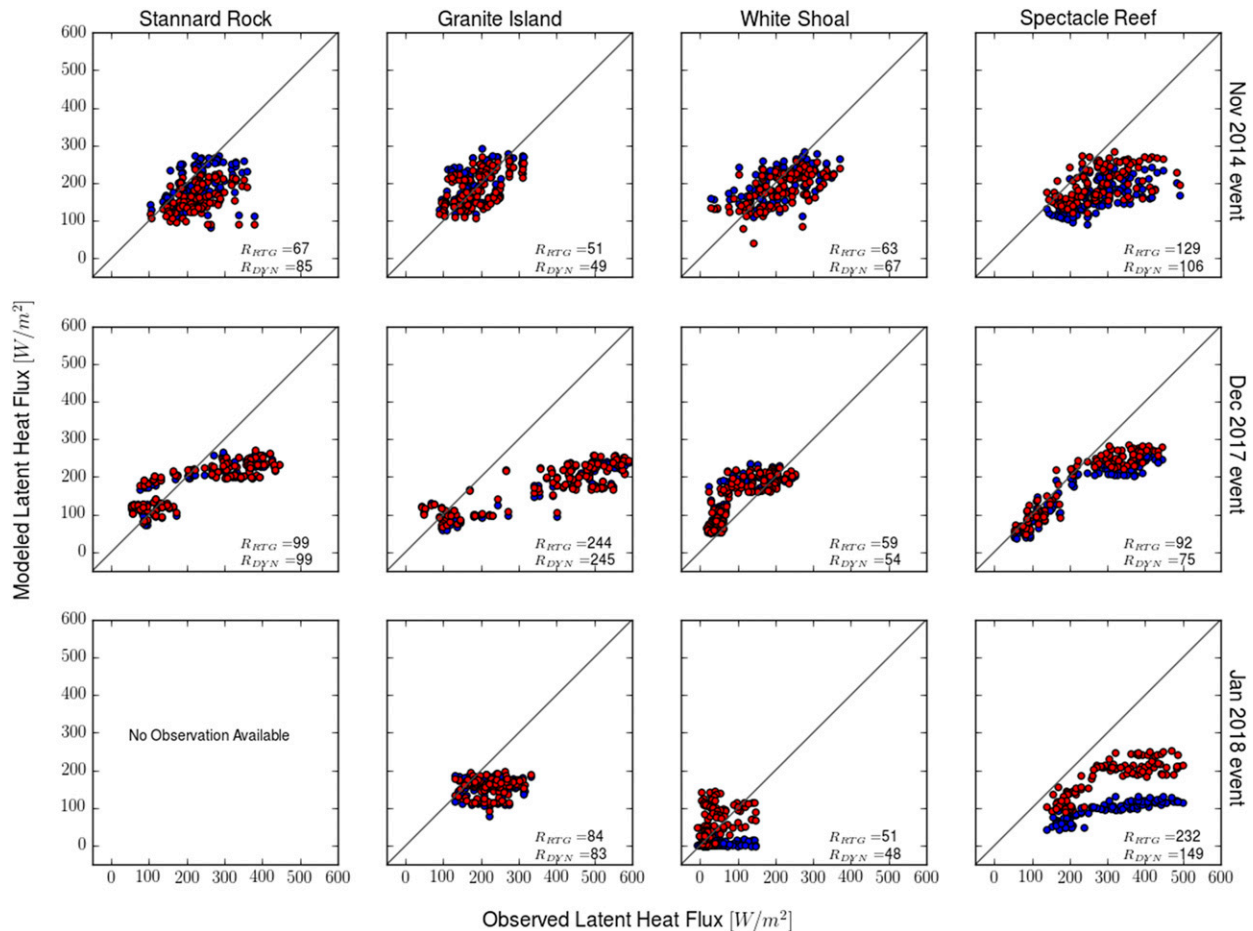


FIG. 8. As in Fig. 7, but for the turbulent latent heat flux  $H_L$ .

converged on a solution after one back-and-forth between the FVCOM-CICE and WRF (also see the discussion in section 3a). This fact is beneficial for the operational environment as the one-way linkage essentially requires no or little increase in computational time, as compared to performing multiple iterations, to obtain a converged solution.

The improvements in the model results, with only a minor additional preprocessing resource demand, supports the operational applicability of this one-way linkage system between the FVCOM-CICE and WRF. As part of the research-to-operation (R2O) transitions of GLOFS and HRRR, part of the system was demonstrated on a real-time basis (two cycles per day) for the winter of 2019/20 utilizing the existing experimental GLOFS (based on FVCOM-CICE) and experimental HRRR (based on WRF) for future implementation in operations at NOAA's NOS and NWS, respectively. Leveraging each other's products utilizing the existing data dissemination channels at NOAA would be a logical pathway to co-improve forecast products.

#### 4. Summary and conclusions

As a milestone to future implementations in operational GLOFS and HRRR, this study tested and verified

the improvements in relation to LES forecasts via a one-way coupling between the hydrodynamic-ice model (FVCOM-CICE) and the atmospheric model (WRF). The realistic representation and frequent updates of lake-surface cooling and fractional ice development during the three LES events was achieved by feeding the FVCOM-CICE simulated lake-surface conditions to WRF with a regional configuration of the HRRR, resulting in improved simulations of surface meteorology, turbulent heat fluxes over the lakes, and snow water equivalent downwind of the lakes. The one-way coupling essentially required one iteration (i.e., data back-and-forth) of the WRF and FVCOM-CICE system to reach a converged solution. Thus, the one-way linkage is a practical approach in an operational environment at NOAA, as it requires little increase in computational resource yet can result in improved forecasts of weather and lake conditions.

Based on the results in this study, part of the system employed in this study was tested during the winter of 2019/20 at NOAA's Hydrometeorological Testbed on a real-time basis for the experimental versions of GLOFS and HRRR (or HRRRX) for future implementation in operations to provide operational forecasts at NOAA's NOS and NWS, respectively. This study supports that leveraging each other's data streams from GLOFS and HRRR



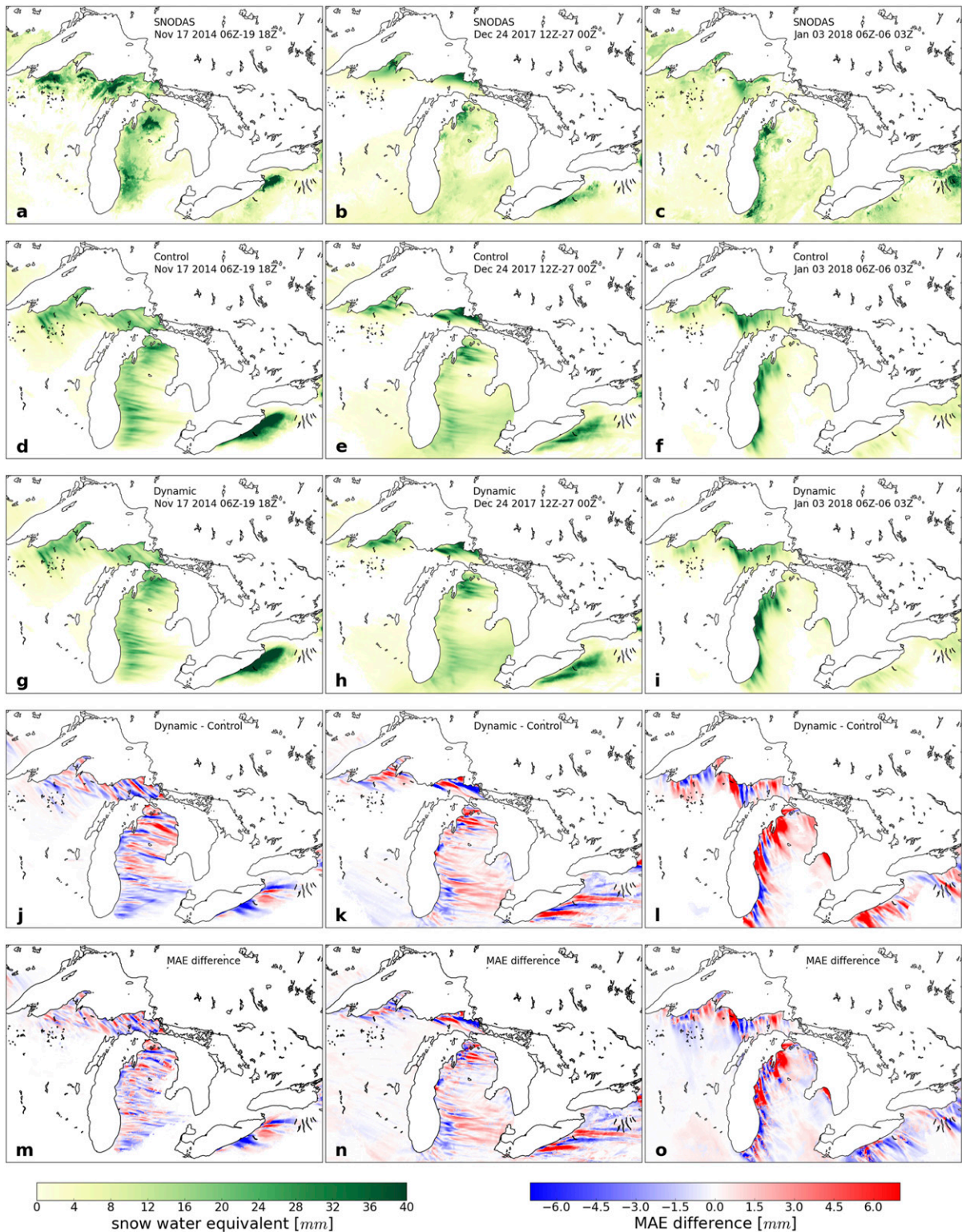


FIG. 9. (a)–(i) Increase of SWE during (left) the November 2014 event, (center) the December 2017 event, (right) and the January 2018 event from SNODAS, the control case, and the dynamic case. (j)–(l) Difference of  $\Delta$ SWE between the control and dynamic case. (m)–(o) Change in mean absolute error from the control and dynamic case where negative and positive values generally indicate improvement and degradation, respectively.

TABLE 2. Threat scores of the SWE simulations for the three downwind areas during the three lake-effect snow events. The three downwind areas (Erie, Michigan, Upper Peninsula) are defined as polygons in Fig. 1. Three values for the SWE thresholds  $S_{\text{thres}}$  used are 10, 20, and 30 kg m<sup>-2</sup>. The scores were not calculated when any of the observed and modeled SWE within a polygon did not reach a threshold value. Bold fonts denote that the score was improved in the dynamic case.

Event name	Threshold	S1 (Erie)		S2 (Michigan)		S3 (Upper Peninsula)		Average	
		Control	Dynamic	Control	Dynamic	Control	Dynamic	Control	Dynamic
Nov 2014	10	0.28	0.27	0.68	<b>0.70</b>	0.62	0.60	—	—
	20	0.20	0.20	0.25	0.23	0.18	<b>0.19</b>	—	—
	30	0.18	<b>0.19</b>	—	—	—	—	—	—
Dec 2017	10	0.49	<b>0.51</b>	0.27	0.27	0.69	<b>0.73</b>	—	—
	20	0.18	0.15	0.24	<b>0.28</b>	0.28	<b>0.33</b>	—	—
	30	—	—	0.03	<b>0.04</b>	0.23	0.23	—	—
Jan 2018	10	0.02	<b>0.13</b>	0.68	0.63	0.44	0.41	—	—
	20	—	—	0.44	0.44	0.34	0.34	—	—
	30	—	—	0.02	<b>0.10</b>	0.02	0.02	—	—
Average	10	—	—	—	—	—	—	0.46	<b>0.47</b>
	20	—	—	—	—	—	—	0.26	<b>0.27</b>
	30	—	—	—	—	—	—	0.10	<b>0.12</b>

and utilizing the existing data dissemination channels would be a logical pathway to co-improve weather, lake, and ice forecasts.

**Acknowledgments.** This study was funded by the NOAA Office of Weather and Air Quality Hydrometeorology Testbed, awarded to the NOAA Great Lakes Environmental Research Laboratory and the Cooperative Institute for Great Lakes Research (CIGLR) through the NOAA Cooperative Agreement with the University of Michigan (NA12OAR4320071). We thank Kyle Klien at NWS (formally a graduate student at the University of Michigan) for assisting with the preliminary meteorological data comparison, as well as two anonymous reviewers for spending time to review the manuscripts and providing the valuable comments. This is GLERL contribution 1954 and CIGLR contribution 1166.

**Data availability statement.** The Great Lakes Evaporation Network (GLEN) data were from the Lake Superior Watershed Partnership website (<https://superiorwatersheds.org/GLEN/>), with data compilation and publication provided by LimnoTech under Award/Contract 10042-400759 from the International Joint Commission (IJC) through a subcontract with the Great Lakes Observing System (GLOS). The statements, findings, conclusions, and recommendations are those of the author(s) and do not reflect the views of GLEN, LimnoTech, the IJC, or GLOS. The Snow Data Assimilation System (SNODAS) data products are available at the National Snow and Ice Data Center website (<https://nsidc.org/data/g02158>). The source codes of the Advanced Research Weather Research and Forecasting (WRF-ARW) Model can be accessible at <https://www2.mmm.ucar.edu/wrf/users/>. The source codes for the Finite Volume Community Ocean Model (FVCOM) can be accessed at <http://fvcom.smast.umassd.edu/FVCOM/Source/code.htm>.

## REFERENCES

- Anderson, E. J., and D. J. Schwab, 2012: Contaminant transport and spill reference tables for the St. Clair River. *Mar. Technol. Soc. J.*, **46**, 34–47, <https://doi.org/10.4031/MTSJ.46.5.4>.
- , and —, 2013: Predicting the oscillating bi-directional exchange flow in the Straits of Mackinac. *J. Great Lakes Res.*, **39**, 663–671, <https://doi.org/10.1016/j.jglr.2013.09.001>.
- , —, and G. A. Lang, 2010: Real-time hydraulic and hydrodynamic model of the St. Clair River, Lake St. Clair, Detroit river system. *J. Hydraul. Eng.*, **136**, 507–518, [https://doi.org/10.1061/\(ASCE\)HY.1943-7900.0000203](https://doi.org/10.1061/(ASCE)HY.1943-7900.0000203).
- , A. J. Bechle, C. H. Wu, D. J. Schwab, G. E. Mann, and K. A. Lombardy, 2015: Reconstruction of a meteotsunami in Lake Erie on 27 May 2012: Roles of atmospheric conditions on hydrodynamic response in enclosed basins. *J. Geophys. Res. Oceans*, **120**, 8020–8038, <https://doi.org/10.1002/2015JC010883>.
- , A. Fujisaki-Manome, J. Kessler, G. A. Lang, P. Y. Chu, J. G. W. Kelley, Y. Chen, and J. Wang, 2018: Ice forecasting in the next-generation Great Lakes Operational Forecast System (GLOFS). *J. Mar. Sci. Eng.*, **6**, 123, <https://doi.org/10.3390/jmse6040123>.
- Assel, R., K. Cronk, and D. Norton, 2003: Recent trends in Laurentian Great Lakes ice cover. *Climatic Change*, **57**, 185–204, <https://doi.org/10.1023/A:1022140604052>.
- Ayon, B. D., 2017: Snow and non-snow events based winter traffic crash pattern analysis and developing lake effect snow induced crash count prediction model. M.S. thesis, Department of Geography, Western Michigan University, 72 pp., [http://scholarworks.wmich.edu/masters\\_theses/1133](http://scholarworks.wmich.edu/masters_theses/1133).
- Bai, X., J. Wang, D. J. Schwab, Y. Yang, L. Luo, G. A. Leshkevich, and S. Liu, 2013: Modeling 1993–2008 climatology of seasonal general circulation and thermal structure in the Great Lakes using FVCOM. *Ocean Modell.*, **65**, 40–63, <https://doi.org/10.1016/j.ocemod.2013.02.003>.
- Barrett, A. P., 2003: National Operational Hydrologic Remote Sensing Center Snow Data Assimilation System (SNODAS) products at NSIDC. NSIDC Special Rep. 11, 19 pp., [http://nsidc.org/pubs/documents/special/nsidc\\_special\\_report\\_11.pdf](http://nsidc.org/pubs/documents/special/nsidc_special_report_11.pdf).
- Benjamin, S. G., and Coauthors, 2016a: A North American hourly assimilation and model forecast cycle: The rapid refresh. *Mon. Wea. Rev.*, **144**, 1669–1694, <https://doi.org/10.1175/MWR-D-15-0242.1>.
- , J. M. Brown, and T. G. Smirnova, 2016b: Explicit precipitation-type diagnosis from a model using a mixed-phase bulk cloud-precipitation microphysics parameterization. *Wea.*

- Forecasting*, **31**, 609–619, <https://doi.org/10.1175/WAF-D-15-0136.1>.
- Blanken, P. D., and Coauthors, 2000: Eddy covariance measurements of evaporation from Great Slave Lake, Northwest Territories, Canada. *Water Resour. Res.*, **36**, 1069–1077, <https://doi.org/10.1029/1999WR900338>.
- , C. Spence, N. Hedstrom, and J. D. Lenters, 2011: Evaporation from Lake Superior: 1. Physical controls and processes. *J. Great Lakes Res.*, **37**, 707–716, <https://doi.org/10.1016/j.jglr.2011.08.009>.
- Briegleb, B. P., 1992: Delta-Eddington approximation for solar radiation in the NCAR community climate model. *J. Geophys. Res.*, **97**, 7603, <https://doi.org/10.1029/92JD00291>.
- Chen, C., R. C. Beardsley, and G. Cowles, 2006: An unstructured grid, finite volume coastal ocean model (FVCOM) system. *Oceanography*, **19**, 78–89, <https://doi.org/10.5670/oceanog.2006.92>.
- , and Coauthors, 2013: An unstructured grid, Finite-Volume Coastal Ocean Model FVCOM User Manual. Tech. Rep. SMAST/UMASSD-13-0701, School Marine Science Technology, University Massachusetts Dartmouth, 416 pp.
- Conrick, R., H. D. Reeves, and S. Zhong, 2015: The dependence of QPF on the choice of boundary- and surface-layer parameterization for a lake-effect snowstorm. *J. Appl. Meteor. Climatol.*, **54**, 1177–1190, <https://doi.org/10.1175/JAMC-D-14-0291.1>.
- Cordeira, J. M., and N. F. Laird, 2008: The influence of ice cover on two lake-effect snow events over Lake Erie. *Mon. Wea. Rev.*, **136**, 2747–2763, <https://doi.org/10.1175/2007MWR2310.1>.
- Fairall, C. W., E. F. Bradley, J. S. Godfrey, G. A. Wick, J. B. Edson, and G. S. Young, 1996a: Cool-skin and warm-layer effects on sea surface temperature. *J. Geophys. Res.*, **101**, 1295–1308, <https://doi.org/10.1029/95JC03190>.
- , —, D. P. Rogers, J. B. Edson, and G. S. Young, 1996b: Bulk parameterization of air-sea fluxes for tropical ocean-global atmosphere coupled-ocean atmosphere response experiment. *J. Geophys. Res.*, **101**, 3747–3764, <https://doi.org/10.1029/95JC03205>.
- , —, J. E. Hare, A. A. Grachev, and J. B. Edson, 2003: Bulk parameterization of air-sea fluxes: Updates and verification for the COARE algorithm. *J. Climate*, **16**, 571–591, [https://doi.org/10.1175/1520-0442\(2003\)016<0571:BPOASF>2.0.CO;2](https://doi.org/10.1175/1520-0442(2003)016<0571:BPOASF>2.0.CO;2).
- Fichot, C. G., K. Matsumoto, B. Holt, M. M. Gierach, and K. S. Tokos, 2019: Assessing change in the overturning behavior of the Laurentian Great Lakes using remotely sensed lake surface water temperatures. *Remote Sens. Environ.*, **235**, 111427, <https://doi.org/10.1016/j.rse.2019.111427>.
- Fujisaki-Manome, A., and Coauthors, 2017: Turbulent heat fluxes during an extreme lake effect snow event. *J. Hydrometeorol.*, **18**, 3145–3163, <https://doi.org/10.1175/JHM-D-17-0062.1>.
- , E. J. Anderson, J. A. Kessler, P. Y. Chu, J. Wang, and A. D. Gronewold, 2020: Simulating impacts of precipitation on ice cover and surface water temperature across large lakes. *J. Geophys. Res. Oceans*, **125**, e2019JC015950, <https://doi.org/10.1029/2019JC015950>.
- Gao, G., C. Chen, J. Qi, and R. C. Beardsley, 2011: An unstructured-grid, finite-volume sea ice model: Development, validation, and application. *J. Geophys. Res.*, **116**, C00D04, <https://doi.org/10.1029/2010JC006688>.
- Gerbush, M. R., D. A. R. Kristovich, and N. F. Laird, 2008: Mesoscale boundary layer and heat flux variations over pack ice-covered Lake Erie. *J. Appl. Meteor. Climatol.*, **47**, 668–682, <https://doi.org/10.1175/2007JAMC1479.1>.
- Grumbine, R., 2014: Automated passive microwave sea ice concentration analysis at NCEP 1196–2012. NCEP Tech. Note, 38 pp., [http://polar.ncep.noaa.gov/mmab/papers/tn321/MMAB\\_321.pdf](http://polar.ncep.noaa.gov/mmab/papers/tn321/MMAB_321.pdf).
- Hjelmfelt, M. R., and R. R. Braham, 1983: Numerical simulation of the airflow over Lake Michigan for a major lake-effect snow event. *Mon. Wea. Rev.*, **111**, 205–219, [https://doi.org/10.1175/1520-0493\(1983\)111<0205:NSOTAO>2.0.CO;2](https://doi.org/10.1175/1520-0493(1983)111<0205:NSOTAO>2.0.CO;2).
- Hunke, E. C., and J. K. Dukowicz, 1997: An elastic–viscous–plastic model for sea ice dynamics. *J. Phys. Oceanogr.*, **27**, 1849–1867, [https://doi.org/10.1175/1520-0485\(1997\)027<1849:AEVPMF>2.0.CO;2](https://doi.org/10.1175/1520-0485(1997)027<1849:AEVPMF>2.0.CO;2).
- , W. H. Lipscomb, A. K. Turner, N. Jeffery, and S. Elliott, 2015: CICE: The Los Alamos Sea Ice Model documentation and software user’s manual. Tech. Rep. LA-CC-06-012, 116 pp.
- Kristovich, D. R., N. F. Laird, and M. R. Hjelmfelt, 2003: Convective evolution across Lake Michigan during a widespread lake-effect snow event. *Mon. Wea. Rev.*, **131**, 643–655, [https://doi.org/10.1175/1520-0493\(2003\)131<0643:CEALMD>2.0.CO;2](https://doi.org/10.1175/1520-0493(2003)131<0643:CEALMD>2.0.CO;2).
- Laird, N. F., D. A. R. Kristovich, and J. E. Walsh, 2003: Idealized model simulations examining the mesoscale structure of winter lake-effect circulations. *Mon. Wea. Rev.*, **131**, 206–221, [https://doi.org/10.1175/1520-0493\(2003\)131<0206:IMSETM>2.0.CO;2](https://doi.org/10.1175/1520-0493(2003)131<0206:IMSETM>2.0.CO;2).
- Lake Carriers’ Association, 2019: Iced out: Study reveals loss of more than \$1 billion due to inadequate icebreaking capabilities on the Great Lakes. Accessed 21 September 2019, <http://www.lcships.com/2019/08/01/iced-out-study-reveals-loss-of-more-than-1-billion-due-to-inadequate-icebreaking-capabilities-on-the-great-lakes/>.
- Large, W. G., and S. Pond, 1981: Open ocean momentum flux measurements in moderate to strong winds. *J. Phys. Oceanogr.*, **11**, 324–336, [https://doi.org/10.1175/1520-0485\(1981\)011<0324:OOMFMI>2.0.CO;2](https://doi.org/10.1175/1520-0485(1981)011<0324:OOMFMI>2.0.CO;2).
- Lenters, J. D., J. B. Anderton, P. D. Blanken, C. Spence, and A. E. Suyker, 2013: Assessing the impacts of climate variability and change on Great Lakes evaporation: Implications for water levels and the need for a coordinated observation network. 2011 Project Reports, D. Brown, D. Bidwell, and L. Briley, Eds., Great Lakes Integrated Science and Assessments (GLISA) Center, 11 pp., [http://glisacclimate.org/media/GLISA\\_Lake\\_Evaporation.pdf](http://glisacclimate.org/media/GLISA_Lake_Evaporation.pdf).
- Mallard, M. S., C. G. Nolte, O. R. Bullock, T. L. Spero, and J. Gula, 2014: Using a coupled lake model with WRF for dynamical downscaling. *J. Geophys. Res. Atmos.*, **119**, 7193–7208, <https://doi.org/10.1002/2014JD021785>.
- Maykut, G. A., and M. G. McPhee, 1995: Solar heating of the Arctic mixed layer. *J. Geophys. Res.*, **100**, 24 691–24 703, <https://doi.org/10.1029/95JC02554>.
- Mellor, G. L., and T. Yamada, 1982: Development of a turbulent closure model for geophysical fluid problems. *Rev. Geophys.*, **20**, 851–875, <https://doi.org/10.1029/RG020i004p00851>.
- , and A. Blumberg, 2004: Wave breaking and ocean surface layer thermal response. *J. Phys. Oceanogr.*, **34**, 693–698, <https://doi.org/10.1175/2517.1>.
- Minder, J. R., W. M. Bartolini, C. Spence, N. R. Hedstrom, P. D. Blanken, and J. D. Lenters, 2020: Characterizing and constraining uncertainty associated with surface and boundary layer turbulent fluxes in simulations of lake-effect snowfall. *Wea. Forecasting*, **35**, 467–488, <https://doi.org/10.1175/WAF-D-19-0153.1>.
- Mironov, D., L. Rontu, E. Kourzenev, and A. Terzhevik, 2010: Towards improved representation of lakes in numerical weather prediction and climate models: Introduction to the



- special issue of Boreal Environment Research. *Boreal Environ. Res.*, **15**, 97–99.
- Mironov, D. V., 2008: Synopsis of FLake routines. Tech. Doc., 15 pp., [http://hirlam.org/index.php/component/docman/doc\\_download/973-synopsis-of-flake-routines-dmitrii-v-mironov?Itemid=157](http://hirlam.org/index.php/component/docman/doc_download/973-synopsis-of-flake-routines-dmitrii-v-mironov?Itemid=157).
- Nakanishi, M., and H. Niino, 2004: An improved Mellor–Yamada Level-3 model with condensation physics: Its design and verification. *Bound.-Layer Meteor.*, **112**, 1–31, <https://doi.org/10.1023/B:BOUN.0000020164.04146.98>.
- , and —, 2009: Development of an improved turbulence closure model for the atmospheric boundary layer. *J. Meteor. Soc. Japan*, **87**, 895–912, <https://doi.org/10.2151/jmsj.87.895>.
- Niziol, T., 1987: Operational forecasting of lake effect snowfall in western and central New York. *Wea. Forecasting*, **2**, 310–321, [https://doi.org/10.1175/1520-0434\(1987\)002<0310:OFOLES>2.0.CO;2](https://doi.org/10.1175/1520-0434(1987)002<0310:OFOLES>2.0.CO;2).
- Notaro, M., A. Zarrin, S. Vavrus, and V. Bennington, 2013: Simulation of heavy lake-effect snowstorms across the Great Lakes basin by RegCM4: Synoptic climatology and variability. *Mon. Wea. Rev.*, **141**, 1990–2014, <https://doi.org/10.1175/MWR-D-11-00369.1>.
- NWS, 2014: Lake Effect Summary: November 17–19, 2014. Buffalo, NY, Weather Forecast Office, [https://www.weather.gov/buf/lake1415\\_stormb.html](https://www.weather.gov/buf/lake1415_stormb.html).
- , 2017: Lake Effect Snow Event Archive. Buffalo, NY, Weather Forecast Office, <https://www.weather.gov/buf/lesEventArchive?season=2017-2018&event=F>.
- , 2018: State Climate Extremes Committee Decision on Erie, Pennsylvania Extreme Snowfall in December 2017. Cleveland, OH, Weather Forecast Office, [https://www.weather.gov/cle/news\\_ErieSnowfall\\_Records\\_Report](https://www.weather.gov/cle/news_ErieSnowfall_Records_Report).
- Oleson, K. W., and Coauthors, 2013: Technical description of version 4.5 of the Community Land Model (CLM). NCAR Tech. Note NCAR/TN-503+STR, 420 pp., <https://doi.org/10.5065/D6RR1W7M>.
- Olson, J. B., and Coauthors, 2019: Improving wind energy forecasting through numerical weather prediction model development. *Bull. Amer. Meteor. Soc.*, **100**, 2201–2220, <https://doi.org/10.1175/BAMS-D-18-0040.1>.
- Plattner, S., D. M. Mason, G. A. Leshkevich, D. J. Schwab, and E. S. Rutherford, 2006: Classifying and forecasting coastal upwellings in Lake Michigan using satellite derived temperature images and buoy data. *J. Great Lakes Res.*, **32**, 63–76, [https://doi.org/10.3394/0380-1330\(2006\)32\[63:CAFCUI\]2.0.CO;2](https://doi.org/10.3394/0380-1330(2006)32[63:CAFCUI]2.0.CO;2).
- Prasad, D. H., J. Wibig, and M. Rzepa, 2010: Numerical modeling of the severe cold weather event over Central Europe (January 2006). *Adv. Meteor.*, **2010**, 1–15, <https://doi.org/10.1155/2010/619478>.
- Reeves, H. D., and D. T. Dawson, 2013: The dependence of QPF on the choice of microphysical parameterization for lake-effect snowstorms. *J. Appl. Meteor. Climatol.*, **52**, 363–377, <https://doi.org/10.1175/JAMC-D-12-019.1>.
- Rowe, M. D., and Coauthors, 2019: Coastal upwelling influences hypoxia spatial patterns and nearshore dynamics in Lake Erie. *J. Geophys. Res. Oceans*, **124**, 6154–6175, <https://doi.org/10.1029/2019JC015192>.
- Samenow, J., 2019: Progress in predictions: With over 40 years of snow forecasting, he wrote the book on East Coast storms. *Washington Post*, 27 November, <https://www.washingtonpost.com/weather/2019/11/27/perspectives-progress-snow-forecasting-washington-man-who-wrote-book-east-coast-storms/>.
- Schwab, D. J., G. A. Leshkevich, and G. C. Muhr, 1999: Automated mapping of surface water temperature in the Great Lakes. *J. Great Lakes Res.*, **25**, 468–481, [https://doi.org/10.1016/S0380-1330\(99\)70755-0](https://doi.org/10.1016/S0380-1330(99)70755-0).
- Shi, Q., and P. Xue, 2019: Impact of lake surface temperature variations on lake effect snow over the Great Lakes region. *J. Geophys. Res. Atmos.*, **124**, 12 553–12 567, <https://doi.org/10.1029/2019JD031261>.
- Skamarock, W. C., and Coauthors, 2008: A description of the Advanced Research WRF version 3. NCAR Tech. Note NCAR/TN-475+STR, 113 pp., <https://doi.org/10.5065/D68S4MVH>.
- Smagorinsky, J., 1963: General circulation experiments with the primitive equations. *Mon. Wea. Rev.*, **91**, 99–164, [https://doi.org/10.1175/1520-0493\(1963\)091<0099:GCEWTP>2.3.CO;2](https://doi.org/10.1175/1520-0493(1963)091<0099:GCEWTP>2.3.CO;2).
- Smirnova, T. G., J. M. Brown, S. G. Benjamin, and J. S. Kenyon, 2016: Modifications to the Rapid Update Cycle land surface model (RUC LSM) available in the Weather Research and Forecasting (WRF) Model. *Mon. Wea. Rev.*, **144**, 1851–1865, <https://doi.org/10.1175/MWR-D-15-0198.1>.
- Spence, C., P. D. Blanken, N. Hedstrom, V. Fortin, and H. Wilson, 2011: Evaporation from Lake Superior: 2. Spatial distribution and variability. *J. Great Lakes Res.*, **37**, 717–724, <https://doi.org/10.1016/j.jglr.2011.08.013>.
- Theeuwes, N. E., G. J. Steeneveld, F. Krikken, and A. A. M. Holtlag, 2010: Mesoscale modeling of lake effect snow over Lake Erie – Sensitivity to convection, microphysics and the water temperature. *Adv. Sci. Res.*, **4**, 15–22, <https://doi.org/10.5194/asr-4-15-2010>.
- Thompson, G., and T. Eidhammer, 2014: A study of aerosol impacts on clouds and precipitation development in a large winter cyclone. *J. Atmos. Sci.*, **71**, 3636–3658, <https://doi.org/10.1175/JAS-D-13-0305.1>.
- Thorndike, A. S., D. A. Rothrock, G. A. Maykut, and R. Colony, 1975: The thickness distribution of sea ice. *J. Geophys. Res.*, **80**, 4501–4513, <https://doi.org/10.1029/JC080i033p04501>.
- Vavrus, S., M. Notaro, and A. Zarrin, 2013: The role of ice cover in heavy lake-effect snowstorms over the Great Lakes basin as simulated by RegCM4. *Mon. Wea. Rev.*, **141**, 148–165, <https://doi.org/10.1175/MWR-D-12-00107.1>.
- Wang, J., J. Kessler, F. Hang, H. Hu, A. H. Clites, and P. Y. Chu, 2018: Analysis of Great Lakes ice cover climatology: Winters 2012–2017. NOAA Tech. Memo. GLERL-171, 24 pp., [https://www.glerl.noaa.gov/pubs/tech\\_reports/glerl-171/tm-171.pdf](https://www.glerl.noaa.gov/pubs/tech_reports/glerl-171/tm-171.pdf).
- Wright, D. M., D. J. Posselt, and A. L. Steiner, 2013: Sensitivity of lake-effect snowfall to lake ice cover and temperature in the Great Lakes region. *Mon. Wea. Rev.*, **141**, 670–689, <https://doi.org/10.1175/MWR-D-12-00038.1>.
- Xiao, C., B. M. Lofgren, J. Wang, and P. Y. Chu, 2016: Improving the lake scheme within a coupled WRF-lake model in the Laurentian Great Lakes. *J. Adv. Model. Earth Syst.*, **8**, 1969–1985, <https://doi.org/10.1002/2016MS000717>.
- Xue, P., D. J. Schwab, and S. Hu, 2015: An investigation of the thermal response to meteorological forcing in a hydrodynamic model of Lake Superior. *J. Geophys. Res. Oceans*, **120**, 5233–5253, <https://doi.org/10.1002/2015JC010740>.
- , J. S. Pal, X. Ye, J. D. Lenters, C. Huang, and P. Y. Chu, 2017: Improving the simulation of large lakes in regional climate modeling: Two-way lake-atmosphere coupling with a 3D hydrodynamic model of the Great Lakes. *J. Climate*, **30**, 1605–1627, <https://doi.org/10.1175/JCLI-D-16-0225.1>.